ILASS Americas, 16th Annual Conference on Liquid Atomization and Spray Systems, Monetery, CA, May 2003

A Posteriori Study of Models for Large Eddy Simulations of Drop-Laden Flows

A. Leboissetier, N. A. Okong'o and Josette Bellan*
Jet Propulsion Laboratory, California Institute of Technology, Pasadena, CA 91109-8099

Abstract

Large Eddy Simulation (LES) is conducted of a three-dimensional temporal mixing layer whose lower stream is initially laden with liquid drops which may evaporate during the simulation. The gas-phase equations are written in an Eulerian frame for two perfect gas species (carrier gas and vapor emanating from the drops), while the liquid-phase equations are written in a Lagrangian frame. The effect of drop evaporation on the gas phase is considered through mass, momentum and energy source terms. Simulations are performed using various LES models previously calibrated on a database obtained from Direct Numerical Simulations (DNS). These LES models consist of Subgrid Scale (SGS) models for the unresolved fluxes of species-mass, momentum and heat, and of filtered source term models expressing the coupling of computational drops with the LES flow field. The SGS flux models considered are the dynamic Smagorinsky (SMD) and the dynamic Gradient (GRD) models, dynamic meaning that the model coefficient is calculated during the LES. Constant-coefficient implementations of these models, despite using DNS-calibrated coefficient values, were found to be numerically unstable for some simulation conditions. While the LES results for the GRD model showed good agreement with the filtered-DNS field it was meant to replicate, the SMD model was overly dissipative and smeared the flow and drop fields to the point that there was virtually no correlation between the LES results and filtered-DNS fields. For the GRD model, a reduction of up to a factor of 32 from the physical drops to computational drops was possible without unduly affecting the degree of agreement between LES and filtered DNS.

Introduction

The Large Eddy Simulation (LES) methodology was conceived for single-phase (SP) flows to decrease computational costs through restricting the resolution to that of the large scales and including the effect of the small scales through models. The LES equations are obtained by spatially filtering the Direct Numerical Simulation (DNS) equation set, as DNS are simulations which compute the entire range of scales typical of turbulent flows. For compressible multi-species flows, this filtering process introduces unresolved momentum, energy and species subgrid scale (SGS) fluxes. Therefore, for SP flows, the necessary SGS models consist of expressions relating the SGS fluxes to the resolved variables. For two-phase (TP) flows with evaporating (liquid) drops, the situation is more complicated because the filter volume contains drops. Assuming that the drops are small enough to be treated as point sources, their evolution depends on the gas-phase flow field, and in turn they affect the gas phase by acting as sources of mass, momentum and energy. Consistency in the goal of decreasing computational costs dictates that not only must the flow resolution be decreased in LES with respect to DNS, but the same concept also must be applied to the ensemble of drops. That is, in LES the drops should not be the physical drops of DNS, but instead should be 'computational' drops representing the effect of several physical drops. Therefore, TP LES requires modeling both the effect of the flow field on the drops (through the drop far-field), and that of the drops on the flow field (through filtered source terms).

We use here SGS-flux and filtered-source-term LES models presented in a recent study [1], in which DNS databases were used to calibrate constant-coefficient SGS-flux models for the flows to be computed here. The models have the intent of introducing a consistent TP flow LES methodology wherein both the number of grid points and that of tracked drops is reduced compared to DNS. The goal of the LES is to replicate the filtered DNS fields produced in Ref. [1].

Highlights of the DNS model

The detailed DNS equations along with the justification of the assumptions embodied in them were described in [1], based on the formulation of [2]. The governing equations are formulated in an Eulerian frame for the gas phase and a Lagrangian frame for the drops. The gas phase consists of two species which are the carrier gas

*Corresponding author: josette.bellan@jpl.nasa.gov.

and the vapor evolving from the drops. The drops are treated as point sources of mass, momentum and energy for the gas phase; this treatment is justified by the dilute (i.e. volumetrically small, $O(10^{-3})$) loading and the size of each particle being much smaller than the Kolmogorov scale.

The mixing layer geometry is illustrated in Fig. 1 where the streamwise (x_1), the cross-stream (x_2), and the spanwise (x_3), coordinates are shown, and the domain lengths are L_1, L_2 and L_3 in each direction. Periodic boundary conditions are used in the x_1 and x_3 directions, and adiabatic slip wall conditions are employed for the x_2 boundaries. The free-stream velocity $U_0 = M_{c,0}a_{C,0}$ is calculated from a specified value of the convective Mach number $M_{c,0}$ based on the carrier gas initial speed of sound $a_{C,0} = \sqrt{R_C T_{C,0} C_{p,C}/C_{v,C}}$ where $T_{C,0}$ is the initial uniform temperature of the carrier gas at the initial uniform pressure; the carrier gas is the sole initial species in the gas phase. The initial vorticity thickness is $\delta_{\omega,0} = \delta_\omega(0)$ where $\delta_\omega(t) = \Delta U_0/\left(\partial\langle u_1\rangle/\partial x_2\right)_{\max}$ with the brackets $\langle\rangle$ denoting averages over homogeneous (x_1, x_3) planes and the velocity difference across the layer is $\Delta U_0 = 2U_0$; the initial mean streamwise velocity has an error-function profile. The specified value of the initial Reynolds number, $\mathrm{Re}_0 = \rho_0 \Delta U_0 \delta_{\omega,0}/\mu$, where ρ_0 is the initial gas density, is used to calculate μ. The thermal conductivity and diffusivity are then computed using this value of μ and specified values of Prandtl and Schmidt numbers of 0.697 (the Lewis number is unity). All thermophysical properties are the same as those employed in the simulations of [3] using air as the carrier gas and decane as the drop liquid.

To promote layer growth, the layer is initially perturbed so as to induce roll-up and pairing. The perturbations, described in [2], specify spanwise and streamwise vorticity fluctuations, with streamwise and spanwise wavelengths in the x_1 and x_3 directions of $\lambda_1 = 7.29\delta_{\omega,0}$ and $\lambda_3 = 0.6\lambda_1$. For all the simulations performed herein, $L_1 = 0.2$ m, $L_1 = 4\lambda_1$, $L_2 = 1.1L_1$ and $L_3 = 4\lambda_3$. The relative amplitudes of the forcing perturbations with respect to the circulations are 10% and 2.25% in the spanwise and streamwise directions, respectively.

The drops are initially distributed randomly throughout the $x_2 < 0$ domain with specified temperature, velocity, number density and size distribution. Initially, all the drops have the same temperature, $T_{d,0}$, and have the same velocity as the gas phase at their location. The mean number density profile is smoothed near the centerline, $x_2 = 0$, using an error function profile. The drop size distribution is initially specified through the drop Stokes number $St = \tau_d \Delta U_0/\delta_{\omega,0}$ whose initial distribution is Gaussian with mean 3 and standard deviation 0.5. The number of drops is determined by the initial mass loading ML_0 (initial ratio of mass of liquid to mass of carrier gas in drop-laden part of domain).

The DNS equations were numerically solved using a fourth-order explicit Runge-Kutta temporal integration for time derivatives and eighth-order central finite differences with tenth-order filtering for spatial derivatives. A fourth-order Lagrange interpolation procedure was used to obtain gas-phase variable values at the drop locations.

Of the several DNS cases simulated in Ref. [1], the present interest is in the simulations that were performed at $\mathrm{Re}_0 = 600$ and ML_0=0.2, denoted TP600a2. This case had $M_{c,0}$=0.35, $T_{C,0}$=375K, ρ_0=0.9415kg/m^3, ΔU_0=271.7m/s, $\delta_{\omega,0}$=6.859$\times 10^{-3}$m, $T_{d,0}$=345K and liquid density of 642kg/m^3. The DNS used 2,993,360 drops and 288$\times$320$\times$176 grid points; at the transitional state which occurred at the nondimensional time ($t^* = t\Delta U_0/\delta_{\omega,0}$) of 105, this layer attained a momentum-thickness Reynolds number $\mathrm{Re}_m = \rho_0 \Delta U_0 \delta_m/\mu$ of 1576, where the momentum thickness δ_m, is calculated as

$$\delta_m = \frac{\int_{x_{2,\min}}^{x_{2,\max}} \left[\theta_1 - \langle\rho u_1\rangle\right]\left[\langle\rho u_1\rangle - \theta_2\right] dx_2}{\left(\theta_1 - \theta_2\right)^2} \qquad (1)$$

with $x_{2,\max} = L_2/2$ and $x_{2,\min} = -L_2/2$ being the slip wall coordinates, $\theta_1 = \langle\rho u_1\rangle_{x_2,\max}$ and $\theta_2 = \langle\rho u_1\rangle_{x_2,\min}$.

LES Methodology

The intent of the LES is to replicate the filtered-DNS fields, while reducing both the number of grid points and the number of computational drops. Therefore, the LES initial condition was the filtered DNS field at $t = 0$. The LES uses one-quarter of the number of points of the DNS in each direction, and the filter width is twice the LES grid spacing (eight times the DNS grid spacing). The LES used the same numerical scheme as the DNS, that is, a fourth-order explicit Runge-Kutta temporal integration for time derivatives and eighth-order central finite differences with tenth-order filtering for spatial derivatives. Using this numerical scheme, all the SGS activity is portrayed by the LES models, with little numerical dissipation.

For the SGS fluxes, we consider three typical models: Smagorinsky (SM), Gradient (GR) and Scale-Similarity (SS). For the constant-coefficient implementations of these models, denoted SMC, GRC and SSC, we used coefficients calibrated on DNS databases at the same Reynolds number [3]. In LES of SP flows, the SMC

and SSC models had poor correlations with the filtered DNS [4], and therefore are not considered here. The GRC model was found to be unstable at a higher mass loading of 0.5, leading to its elimination from the present study. In view of the unsatisfactory performance of the constant-coefficient models, we implemented dynamic versions of the Smagorinsky and Gradient models, denoted SMD and GRD respectively, in which the model coefficient is computed from the LES field. Further details on the SGS-flux models are presented in Ref. [4].

To study the issue of reducing the number of computed drops, we consider that each computational drop represents a fixed number of physical drops. That is, if the number of real drops is N_α and the number of computational drops is N_β, then each computational drop β represents N_R drops, where $N_R = N_\alpha/N_\beta$ is the ratio between the number of physical drops and the number of computational drops. The filtered source terms are then computed for the N_β drops, and scaled by N_R leading to

$$\bar{S}_m\left(\psi_{f,m}\left(\bar{\phi}\right),\bar{Z}\right) = N_R \sum_\beta \frac{1}{V_f}\left[S_d\left(\psi_{f,m}\left(\bar{\phi}\right),\bar{Z}\right)\right]_\beta \tag{2}$$

where $\bar{Z}$ is the computational drop field, $S_d = \{S_{I,d}, S_{II,i,d}, S_{III,d}\}$ are the source terms in the continuity, momentum and energy equations, $\bar{S} = \left\{\bar{S}_I, \bar{S}_{II,i}, \bar{S}_{III}\right\}$ is the filtered source term and V_f is the filtering volume of width $\bar{\Delta}$ containing β drops. The LES-field vector of conservative variables is denoted $\bar{\phi}$ and $\psi_{f,m}$ is the model for the drop far-field primitive variables. For the LES in this study, N_R, the ratio of physical drops to computational drops, was varied from 1 to 64.

Evolution of the global quantities

Figure 2 presents the evolution of the global quantities for case TP600a2 with $N_R = 8$, for LES utilizing the GRD and SMD models. The LES results are compared to DNS and F-DNS results; here F-DNS refers to the DNS flow field first filtered at the LES filter width and then having grid points extracted at the LES grid spacing, in conjunction with a reduced drop field using $N_R = 8$. For both LES, the layers roll up and pair twice. The growth of the layers as measured by the momentum thickness δ_m (Fig. 2(a)), and the global mixing as measured by the product thickness δ_P (Fig. 2(b)) are the same on the DNS and F-DNS fields;

$$\delta_P = \int_0^{L_3}\int_{x_{2,\min}}^{x_{2,\max}}\int_0^{L_1} \rho\left[2\min\left(Y_V, Y_C\right)\right] dx_1 dx_2 dx_3, \tag{3}$$

where Y_V and Y_C are the vapor and carrier gas mass fractions respectively. The momentum thickness is well predicted by the GRD model but only until the second pairing time, after which the layer growth is under-predicted. For the SMD model, δ_m is less than the F-DNS value throughout the layer evolution, although for $t^* \gtrsim 80$, the SMD δ_m is larger than the GRD value and is in between the F-DNS value and the GRD value. At the transition time of $t^* = 105$, the SMD value of 2.229 is within 10% of the F-DNS value of 2.485, while the GRD value of 2.113 is 15% lower than the F-DNS value. The product thickness is better predicted by the SMD model, although the GRD prediction is very close to the F-DNS, with a slight over-prediction from the GRD model between the first pairing time and the transition time.

Although the SMD and GRD models seem comparable when considering the momentum and product thicknesses, dramatic differences emerge when the vorticity activity of the layers is examined. The global positive spanwise vorticity ($\langle\langle\omega_3^+\rangle\rangle$ in Fig. 2(c)), which is initially null, is a measure of activity in the resolved small scales, while the enstrophy ($\langle\langle\omega_i\omega_i\rangle\rangle$ in Fig. 2(d)) is related to stretching and tilting which is an important mechanism for turbulence production. The F-DNS field expectably has much less vorticity activity than the DNS field, since filtering reduces the magnitude of the gradients of the DNS field. For both $\langle\langle\omega_3^+\rangle\rangle$ and $\langle\langle\omega_i\omega_i\rangle\rangle$, the SMD model leads to a dearth of activity with very little increase in either quantity. In contrast, the GRD model is quantitatively much closer to the F-DNS than is the SMD model. Furthermore, the GRD model qualitatively captures the variation of the F-DNS, although the peak in $\langle\langle\omega_3^+\rangle\rangle$ and $\langle\langle\omega_i\omega_i\rangle\rangle$ occurs somewhat sooner than it should. The indications are that the SMD model is too dissipative to calculate small turbulent structures similar to the filtered DNS. Detailed scrutiny of the spanwise vorticity distribution in the between-the-braid (x_1, x_2) plane at the transition time [4] confirms that the SMD model dampens the smallest instabilities developing in the mixing layer and that only the GRD model is able to match the filtered DNS and correctly describe the turbulence activity of the resolved small scales.

Finally, the drop-ensemble-average temperature $\langle\langle T_d\rangle\rangle$ and diameter-squared $\langle\langle d^2\rangle\rangle$ (Figs. 2(e) and 2(f)) of physical (DNS) drops are closely followed by the LES using both the SMD and the GRD models. For the F-DNS field, it can be seen that $\langle\langle T_d\rangle\rangle$ and $\langle\langle d^2\rangle\rangle$ match those of the full (DNS) drop field. For $\langle\langle T_d\rangle\rangle$, the GRD model overlaps the DNS until $t^* \simeq 80$, approximately the time of the second pairing, after which it is smaller. The SMD results under-predict the F-DNS until $t^* \simeq 80$,

overlap for $60 \lesssim t^* \lesssim 80$ and thereafter again underpredict the F-DNS $\langle\langle T_d \rangle\rangle$. The GRD and SMD models are comparable at the later times after $t^* \simeq 80$. As elaborated in Ref. [5], the oscillations in $\langle\langle T_d \rangle\rangle$ are due to the competing effects of heating, which transfers energy from the gas phase, and evaporation, which releases energy into the surrounding gas. In considering $\langle\langle d^2 \rangle\rangle$, it is seen that, because this is an ensemble-average result, the drops do not follow the single-drop d^2 law (linear decay); after an initial period of high rate of $\langle\langle d^2 \rangle\rangle$ decrease, this rate subsides as the increasing Y_V impedes evaporation. The SMD model is slightly superior to the GRD model, although both models give excellent predictions of $\langle\langle d^2 \rangle\rangle$.

The global quantities show that the momentum and product thicknesses, and the average drop temperature and diameter-squared are slightly better predicted by the SMD model than by the GRD model. However, this superiority of the SMD model is negated by its poor predictions of the small scale activity, for both the positive spanwise vorticity and the enstrophy. Furthermore, as shown below, despite having good predictions for the product thickness and the drop-average quantities, the SMD model fails to capture the details of the spatial distribution of the drops.

Flow visualizations of the vapor mass fraction and of the drop number density

The vertical mixing (i.e. in the x_2 direction) of the vapor and drops can be assessed for case TP600a2 at transition time from analysis of Fig. 3, which shows the vapor mass fraction (Y_V) and the drop number density (ρ_n) for the F-DNS and the SMD and GRD LES, in the between-the-braid plane. The F-DNS Y_V plot (Fig. 3(a)) shows the ultimate vortex as the largest structure, with complex small scale activity within it. Likewise, ρ_n (Fig. 3(b)) shows complex drop organization, with regions of high ρ_n within the layer; these regions are seen to correspond to the highest Y_V regions inside the layer. The highest Y_V overall occurs in the lower stream, which has a nearly uniform drop distribution at a value intermediate of the ρ_n range. In considering the SMD model prediction, both Y_V (Fig. 3(c)) and ρ_n (Fig. 3(d)) show a qualitatively different aspect than the F-DNS; the SMD model seems to have captured the ultimate vortex, but it is devoid of any small-scale activity, and the drops seem to be mostly concentrated at the edges of this vortex with few drops within the layer. Therefore, the indications are that the SMD model is an inadequate SGS model, since it fails at its primary purpose of reproducing the small-scale motions of the flow. In contrast, the GRD model is seen to have predictions that are both qualitatively correct and quantitatively close compared to the F-DNS field. The Y_V field (Fig. 3(e)) shows both large-scale and small-scale activity, although expectably smeared due to the coarser LES grid. Likewise, ρ_n (Fig. 3(f)) follows the F-DNS in both the lower stream distribution as well as the regions of high ρ_n within the layer.

To ascertain the effect of computational-drop modeling, illustrated in Fig. 4 is the effect of decreasing the number of computational drops when using the GRD model. Notably, compared to the $N_R = 8$ result (previously depicted in Figs. 3(e) and 3(f)), no new qualitative features are observed in either the Y_V or the ρ_n plots when the number of computational drops is equal to the number of physical drops ($N_R = 1$ in Figs. 4(a) and 4(b)), although the drop distribution in the lower stream is more uniform for $N_R = 1$. The $N_R = 16$ LES (not shown) is virtually the same as the $N_R = 8$ result. The accuracy of the GRD model shows no significant degradation when the number N_R is increased to 32 (Figs. 4(c) and 4(d)). Finally, for $N_R = 64$, the aspect of the layer is still qualitatively correct, however a low Y_V region, that does not appear in the lower N_R LES, is seen in the lower stream (Fig. 4(e)), corresponding to a low ρ_n region (Fig. 4(f)). Therefore, for the simulations we have considered, the indications are that the maximum drop reduction should be $N_R = 32$; compared to the DNS, the drop reduction of 32 will be less than the reduction in the number of grid points, which is 64-fold.

Conclusions

LES have been conducted of a three-dimensional temporal mixing layer whose lower stream is initially laden with liquid drops which may evaporate during the simulation. The gas-phase equations are written in an Eulerian frame for two perfect gas species (carrier gas and vapor emanating from the drops), while the liquid-phase equations are written in a Lagrangian frame. The effect of drop evaporation on the gas phase is considered through mass, momentum and energy source terms. LES have been performed with various numbers of computational drops and with two different SGS-flux models, namely, dynamic variants of the Smagorinsky model (SMD) and of the Gradient model (GRD). Only dynamic models were considered for *a posteriori* analysis, because constant-coefficient models using coefficients calibrated on a DNS database were found to be unstable.

The SMD model was found to be excessively dissipative, and yielded distributions of vapor mass fraction and drop number density that had poor visual correlation with the filtered DNS flow fields. The GRD model over-

all demonstrated closer results to the filtered DNS database. Not only was the GRD model stable in every case and able to calculate small scales similar in size to the filtered DNS, but in contrast to the SMD model, it also proved to closely match the temporal evolution of the resolved small scales of the mixing layer, and the spatial distribution of the vapor mass fraction and of the drops. The accuracy of the GRD model showed no significant degradation when the ratio of physical drops to computational drops was increased up to 32, along with a 64-fold reduction in grid points compared to the DNS. Therefore the GRD model seems promising for future LES of flows laden with evaporating drops.

Acknowledgements

This work was conducted at the Jet Propulsion Laboratory of the California Institute of Technology under the sponsorship of the U.S. Department of Energy (DOE), with Mr. Pete Devlin and Ms. Roxanne Danz (DOE Headquarters), and Mr. D. Hooker (DOE Golden Center) serving as contract monitors, under an agreement with the National Aeronautics and Space Administration. Computations were performed on the SGI Origin 2000 at the JPL Supercomputing Center.

References

[1] Okong'o, N., and Bellan, J., Consistent large eddy simulation of a temporal mixing layer laden with evaporating drops. Part I: Direct numerical simulation, formulation and *a priori* analysis, submitted to *Journal of Fluid Mechanics* (2003).

[2] Miller, R. S., and Bellan, J., *Journal of Fluid Mechanics* 384:293–338 (1999).

[3] Miller, R. S., and Bellan, J., *Physics of Fluids* 12(3):650–671 (2000).

[4] Leboissetier, A., Okong'o, N., and Bellan, J., Consistent large eddy simulation of a temporal mixing layer laden with evaporating drops. Part II: *A posteriori* modeling, submitted to *Journal of Fluid Mechanics* (2003).

[5] Le Clercq, P. and Bellan, J. Direct numerical simulation of a transitional temporal mixing layer laden with multicomponent-fuel evaporating drops using continuous thermodynamics, Submitted to *Journal of Fluid Mechanics* (2002).

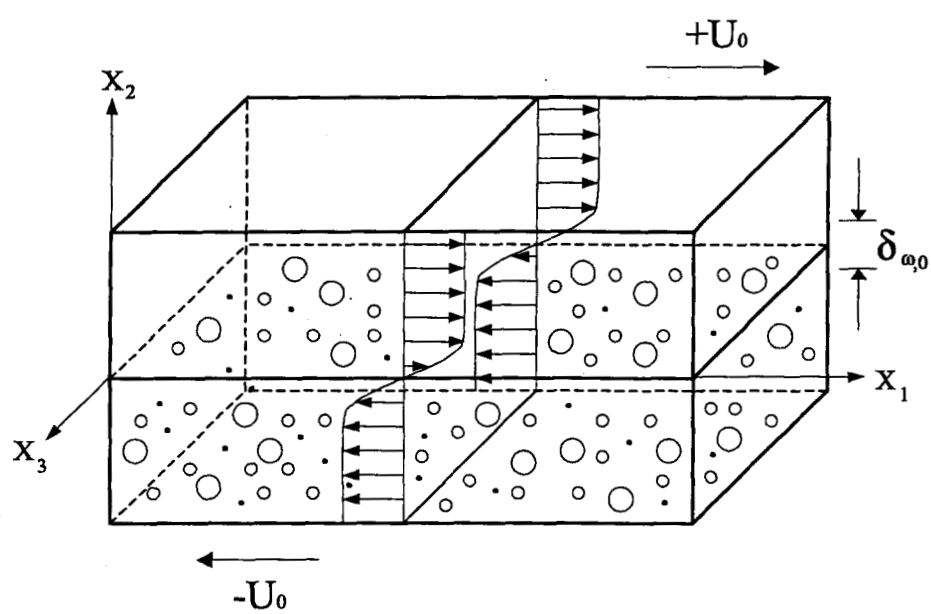

Figure 1: Mixing layer configuration

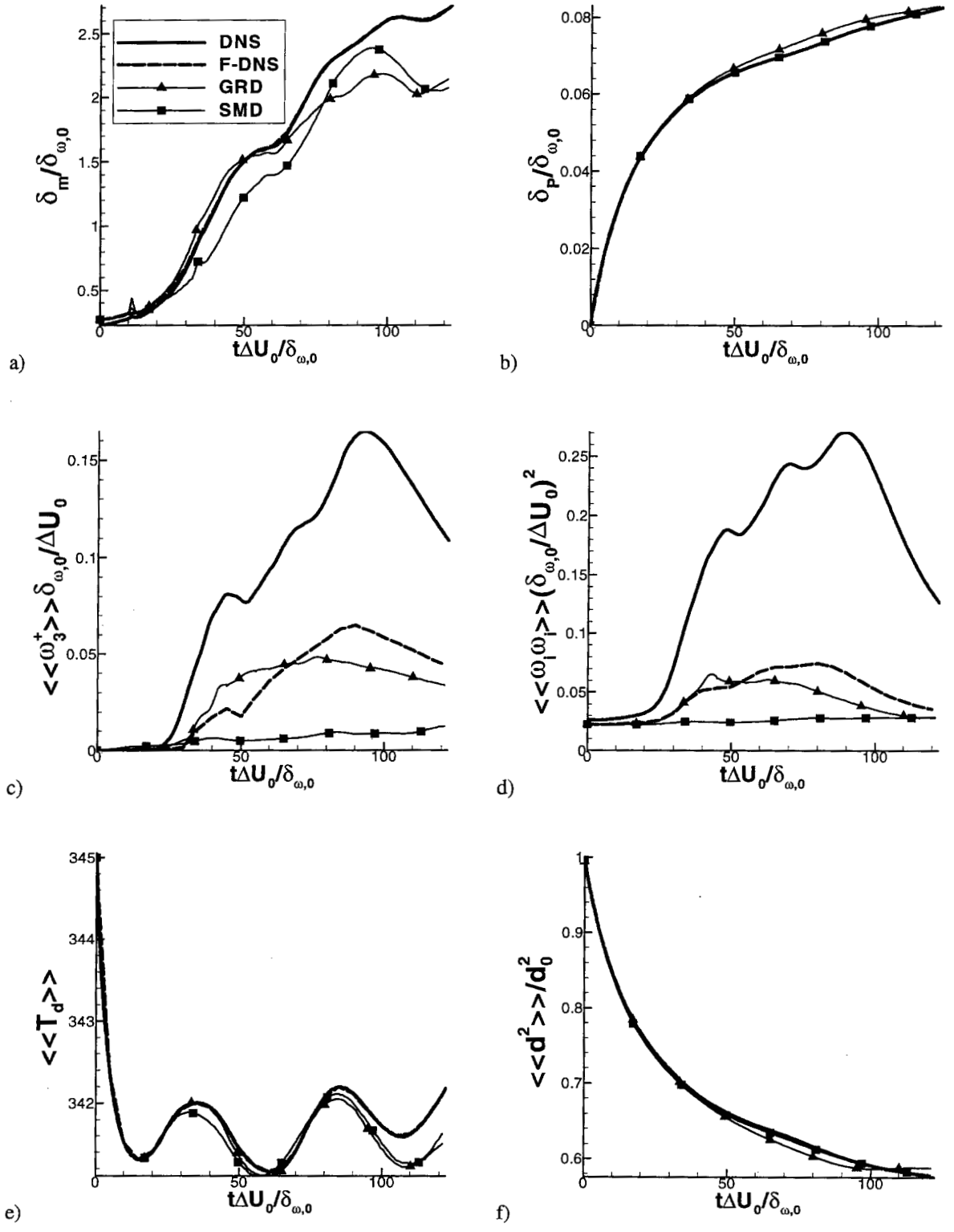

Figure 2: Global evolution for TP600a2 for the DNS, the filtered DNS (F-DNS) and LES using the SMD and GRD models: (a) momentum thickness, (b) product thickness, (c) positive spanwise vorticity, (d) enstrophy, (e) average drop temperature, and (f) average drop diameter-squared.

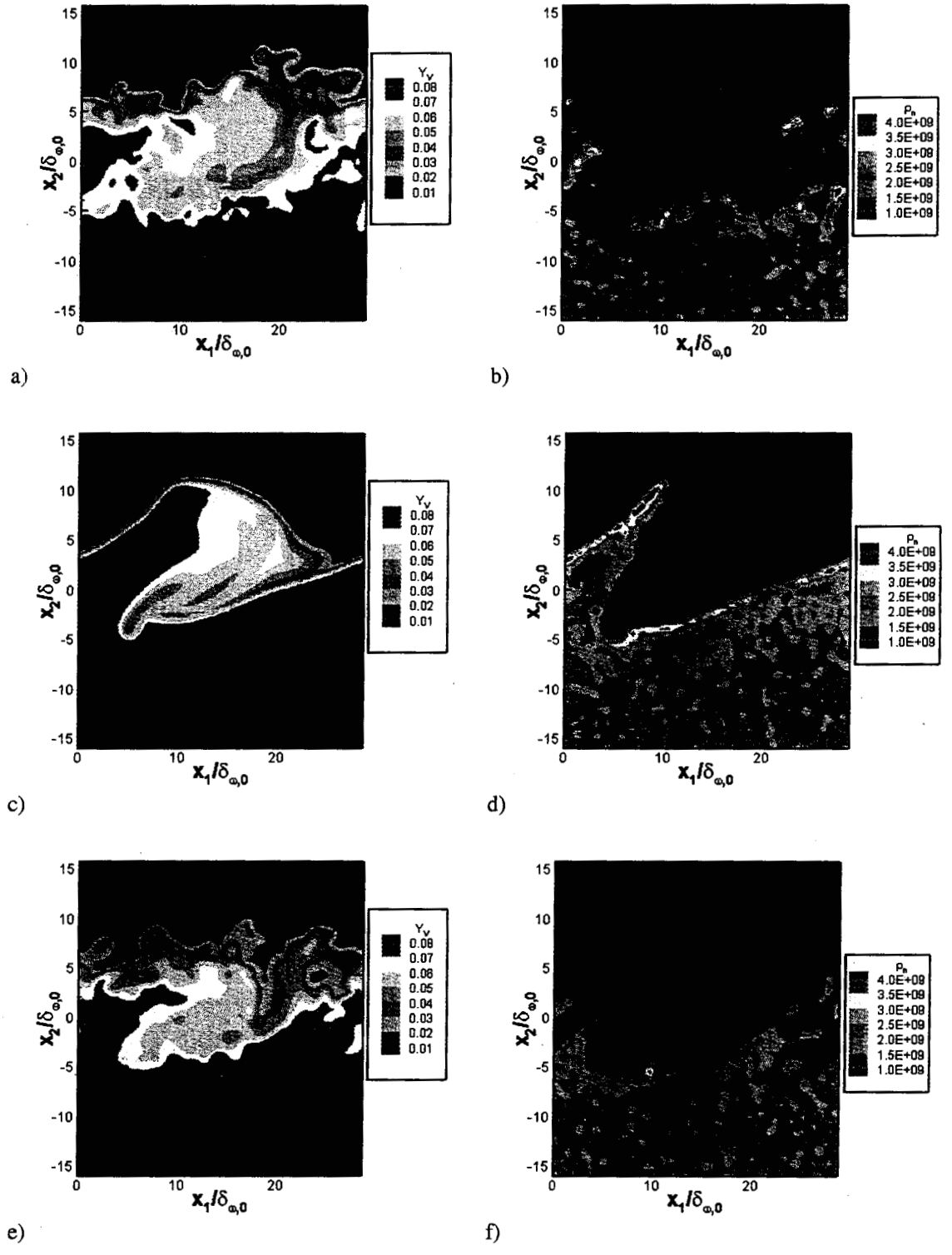

Figure 3: Vapor mass fraction (left) and drop number density (m^{-3}) (right) for TP600a2 in the between-the-braid plane (x_3/L_3=0.5) at t^*_{trans}=105 for $N_R = 8$: (a,b) F-DNS, (c,d) SMD LES and (e,f) GRD LES.

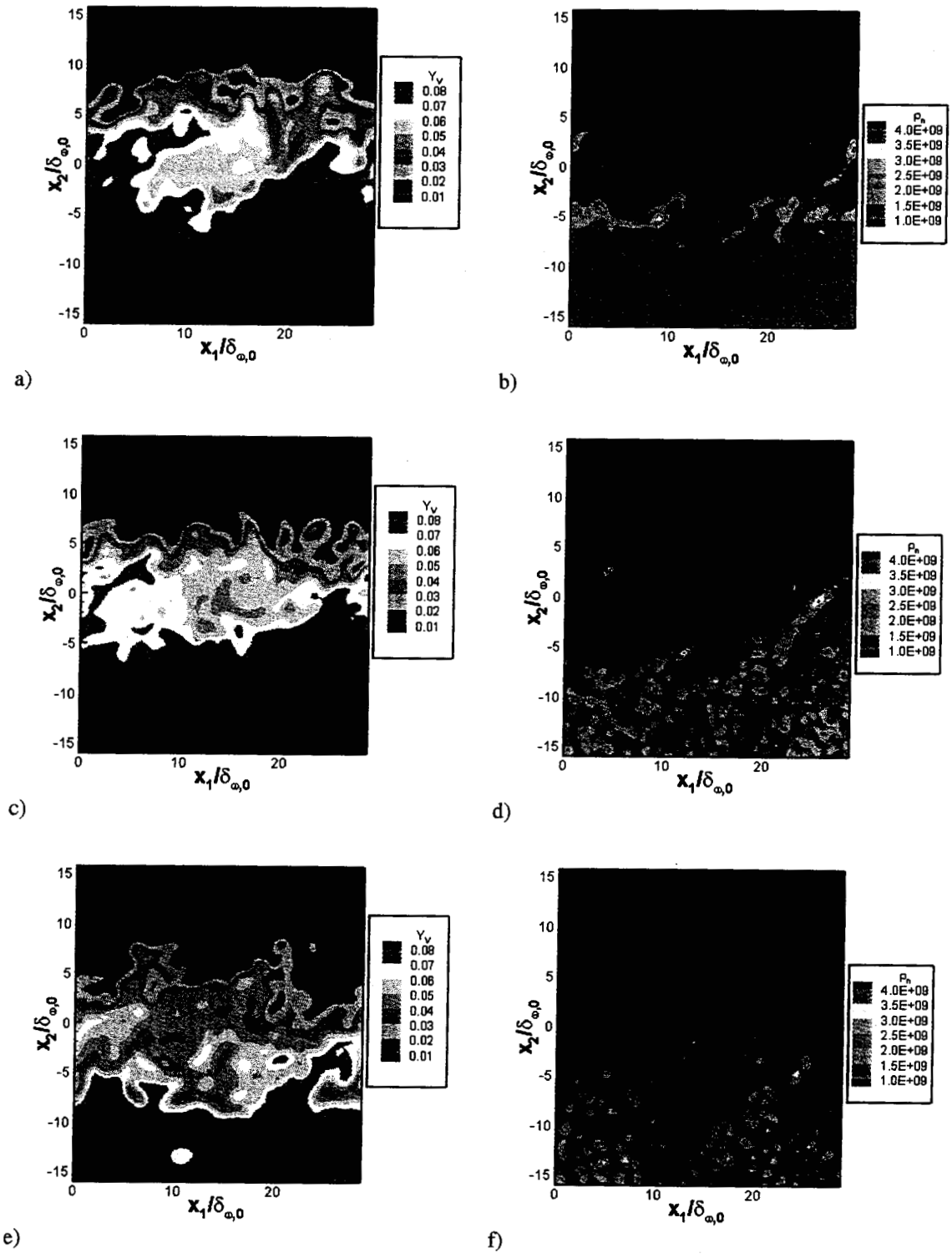

Figure 4: Vapor mass fraction (left) and drop number density (m^{-3}) (right) distribution for TP600a2 in the between-the-braid plane ($x_3/L_3 = 0.5$) at $t^*_{trans} = 105$: LES using the GRD model with (a,b) $N_R = 1$, (c,d) $N_R = 32$, and (e,f) $N_R = 64$.